

OPTICAL FIBRES

PACS numbers: 42.81.Cn; 78.60.Lc
DOI: 10.1070/QE2015v045n01ABEH015624

Luminescence properties of IR-emitting bismuth centres in SiO_2-based glasses in the UV to near-IR spectral region

E.G. Firstova, I.A. Bufetov, V.F. Khopin, V.V. Vel'miskin, S.V. Firstov, G.A. Bufetova, K.N. Nishchev, A.N. Gur'yanov, E.M. Dianov

Abstract. **We have studied UV excitation spectra of IR luminescence in bismuth-doped glasses of various compositions and obtained energy level diagrams of IR-emitting bismuth-related active centres (BACs) associated with silicon and germanium atoms up to ~5.2 eV over the ground level. A possible energy level diagram of the BACs in phosphosilicate glass has been proposed. The UV excitation peaks for the IR luminescence of the BACs in the glasses have been shown to considerably overlap with absorption bands of the Bi^{3+} ion, suggesting that Bi^{3+} may participate in BAC formation.**

Keywords: *optical fibre, bismuth, bismuth centres, luminescence.*

1. Introduction

Studies of bismuth-doped glasses and optical fibres have led to the advent of a variety of new efficient lasers emitting in the range 1.15–1.75 μm [1–3], fibre amplifiers [4, 5] and superluminescent light sources [6, 7]. The doping of glasses of certain compositions with a small amount (~0.1 wt %) of bismuth results in the formation of IR-emitting bismuth-related active centres (BACs), which determine the luminescence and gain properties of the active medium. There is still no physical model capable of adequately interpreting at least the major known experimental findings on the BACs, so gaining new reliable data on the BACs is a necessary condition for further progress in this area of research.

As shown earlier (see e.g. Refs [8–10]), the properties of the BACs depend significantly on glass composition. Firstov et al. [11] studied in detail the luminescence spectra of bismuth-doped silica, germanate, phosphosilicate and aluminosilicate glass fibres at low bismuth concentrations (within 0.1 wt %), characteristic of efficient bismuth-doped fibre lasers. As a result, the silica fibre free of other impurities was shown to contain only one type of BAC*, which can be thought of as an IR-emitting bismuth centre associated with silicon (Si-BAC). The BACs in the bismuth-doped germanate glass showed other luminescence properties, due to the presence of germanium (Ge-BACs). Moreover, the germanate fibre, whose core contained a small amount of SiO_2, showed a relatively weak Si-BAC luminescence. Similarly, phosphosilicate and aluminosilicate glasses contained P-BACs and Al-BACs, respectively, in combination with Si-BACs (particularly clear evidence for the presence of Si-BACs in bismuth-doped aluminosilicate glass was provided by Dvoyrin et al. [13]). To date, three-dimensional (3D) luminescence (excitation–emission) spectra of the BACs have only been measured at excitation wavelengths from 450 to 1600 nm [11]. This has made it possible to determine the energy position of the three lowest excited-state levels of the Si-BAC and Ge-BAC.

In this study, to determine the energy position of higher BAC levels the luminescence properties of the BACs were investigated at excitation wavelengths from 250 to 900 nm, which allowed us (with the use of previous results [11]) to obtain 3D luminescence (excitation–emission) spectra of the bismuth-doped glasses in a wide wavelength range (from 250 to 1600 nm).

2. Samples and characterisation techniques

BACs in glasses that have already been shown to offer efficient lasing are of most interest. In view of this, we studied fibre preforms with bismuth-doped silica, germanosilicate, phosphosilicate and aluminosilicate glass cores. All the preforms had pure SiO_2 claddings (produced using substrate tubes from Heraeus 300 glass). In the case of a pure SiO_2 core, the preform had an additional, reflective, fluorine-doped SiO_2 layer [14]. Table 1 lists the samples and fabrication techniques. The bismuth concentration in all the samples was under 0.1 wt % (detection limit of our analytical equipment), so it is not indicated.

At present, there are no readily available bright UV sources in the range 250–450 nm for the excitation of single-mode fibres (such as, e.g., the supercontinuum source used by Firstov et al. [11]). Because of this, in the present study we measured luminescence spectra of the fibre preforms with an FLS920 fluorescence spectrometer (Edinburgh Instruments, United Kingdom) at excitation wavelengths in the range

E.G. Firstova, V.V. Vel'miskin, S.V. Firstov, E.M. Dianov Fiber Optics Research Center, Russian Academy of Sciences, ul. Vavilova 38, 119333 Moscow, Russia; e-mail: kilena85@mail.ru, fir@fo.gpi.ru;
I.A. Bufetov Fiber Optics Research Center, Russian Academy of Sciences, ul. Vavilova 38, 119333 Moscow, Russia; Moscow Institute of Physics and Technology (State University), Institutskii per. 9, 141700 Dolgoprudnyi, Moscow region, Russia;
V.F. Khopin, A.N. Gur'yanov G.G. Devyatykh Institute of Chemistry of High-Purity Substances, Russian Academy of Sciences, ul. Tropinina 49, 603950 Nizhnii Novgorod, Russia;
G.A. Bufetova A.M. Prokhorov General Physics Institute, Russian Academy of Sciences, ul. Vavilova 38, 119991 Moscow, Russia;
K.N. Nishchev N.P. Ogarev Mordovia State University, Bol'shevistkaya ul. 68, 430005 Saransk, Russia

Received 15 July 2014
Kvantovaya Elektronika **45** (1) 59–65 (2015)
Translated by O.M. Tsarev

* It is worth noting that the assumption that silica glass contains several distinct types of BACs [12] is inconsistent with both previous [11] and present results.

Table 1. Designations, compositions and preparation techniques of the glasses.

Glass	Composition	Preparation technique
SBi	100% SiO_2 (+Bi)	Powder-in-tube [14]
GSBi	5% GeO_2 + 95% SiO_2 (+ Bi)	MCVD
ASBi	3% Al_2O_3 + 97% SiO_2 (+ Bi)	MCVD
PSBi	10% P_2O_5 + 90% SiO_2 (+ Bi)	MCVD

250–900 nm. The samples for the measurements were cut across the preform axis and were disk-shaped. Their faces were polished, and their thickness was varied from 0.1 to 2 mm in our experiments. The core, located on the preform axis, had a diameter of ~1.5 mm, and the preform diameter was ~10 mm.

Preforms and fibres drawn out from them may generally differ in luminescence properties because, in contrast to preforms, fibres are subjected to a number of additional processing steps, including several heatings to ~2000 °C, followed by cooling. For example, Zlenko et al. [15] observed changes in luminescence properties during drawing of bismuth-doped holey optical fibres (the properties of the core were influenced by the oxygen present in the holes adjacent to the fibre core). The measurements on the samples indicated in Table 1 showed that the luminescence spectra of the fibre preforms were essentially identical to those of single-mode fibres at excitation wavelengths in the range 450–900 nm. This led us to assume that the luminescence spectra of the preforms and fibres were identical (or differed only slightly) in the wavelength range 250–2000 nm.

Below, experimental data obtained in this study and previously [11] are presented jointly as luminescence intensity I_{lum} vs. excitation wavelength (λ_{ex}) and emission wavelength (λ_{em}). Each 3D luminescence (excitation–emission) spectrum (3D LS) was obtained using more than a hundred conventional, two-dimensional luminescence spectra taken at λ_{ex} intervals of 10 nm and ensures very compact representation of the information. Such 3D graphs clearly show both luminescence bands and the excitation regions for each observed band.

The measured luminescence intensity was corrected for the spectral sensitivity of the detection channel and normalised to the excitation power at each wavelength. The λ_{ex} scan step (10 nm) in the measurements determines primarily the accuracy of wavelength representation in the 3D LS. All the measurements were made at room temperature.

In addition, we measured the optical absorption spectra of the preforms in the UV spectral region at wavelengths from 190 to 350 nm. The UV loss was measured on a Shimadzu UV-3101PC spectrophotometer using the same polished platelets, cut perpendicular to the preform axis.

3. Results

3.1. UV absorption in the bismuth-doped glasses

Figure 1a shows the measured absorption spectra of the preforms in the range 190–350 nm. All the samples (except for GSBi) have an absorption band centred near 220–240 nm (which will be referred to as Ab), due to the presence of bismuth atoms. Indeed, there is no such band in the spectrum of bismuth-free preforms of the same composition: the absorption in them does not exceed 1 dB mm^{-1} (for comparison, Fig. 1a shows the absorption spectrum of silica glass prepared by the same procedure as in this study, but free of bismuth). The GSBi sample has an order of magnitude stronger absorption band centred at 242 nm, which arises from germanium-related oxygen-deficient centres (GODCs) [16] and obscures the bismuth-related band.

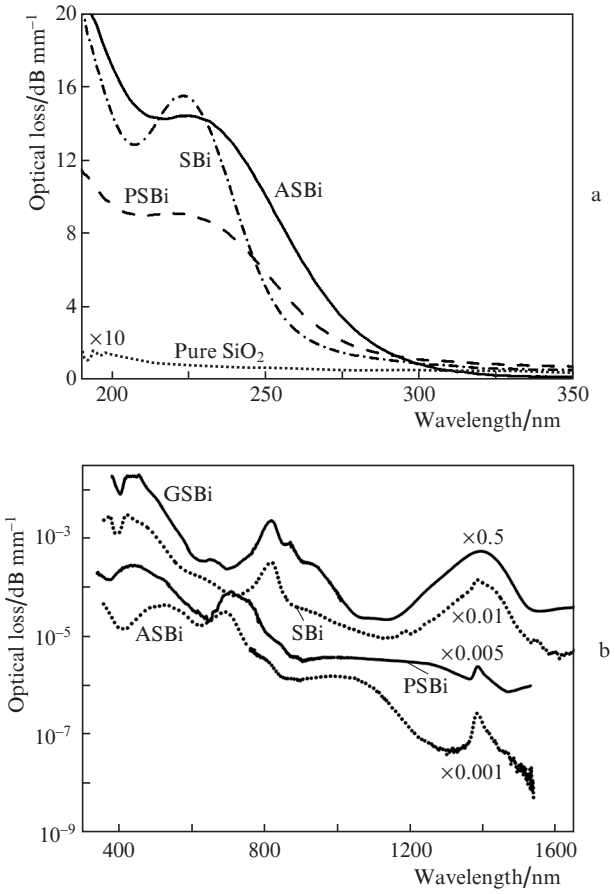

Figure 1. (a) UV absorption spectra of the preforms and (b) visible/IR absorption spectra of the fibres.

It is seen in Fig. 1a that, in all cases, the Ab band is located on the long-wavelength side of a stronger absorption band, which seems to peak in the vacuum UV region. As a result, the peak position of the Ab band is rather difficult to determine when the absorption spectrum is measured only to 190 nm (the limit of the working range of our spectrophotometer). There is ample evidence (see e.g. Ref. [17]) that the Ab band arises from the Bi^{3+} $^3P_1 \rightarrow {}^1S_0$ transition. A similar band is present in the spectra of the Tl^+ and Pb^{2+} ions ($d^{10}s^2$). Moreover, there is a widely used technique for assessing the redox properties of glasses from the shift of the Ab absorption band as a function of glass composition at low bismuth, thallium or lead concentrations (see Duffy [18] and references therein). Thus, the SBi, PSBi and ASBi samples have absorption bands of trivalent bismuth in the range 220–240 nm. Figure 1b shows absorption spectra of the fibres (Table 1) in the visible and IR spectral regions. The spectra were taken from previous reports [2, 11], where one can find interpretation of the data. Note that the Ab band corresponds to the lowest energy Bi^{3+} transition, so this ion has no absorption bands in the visible or IR spectral region.

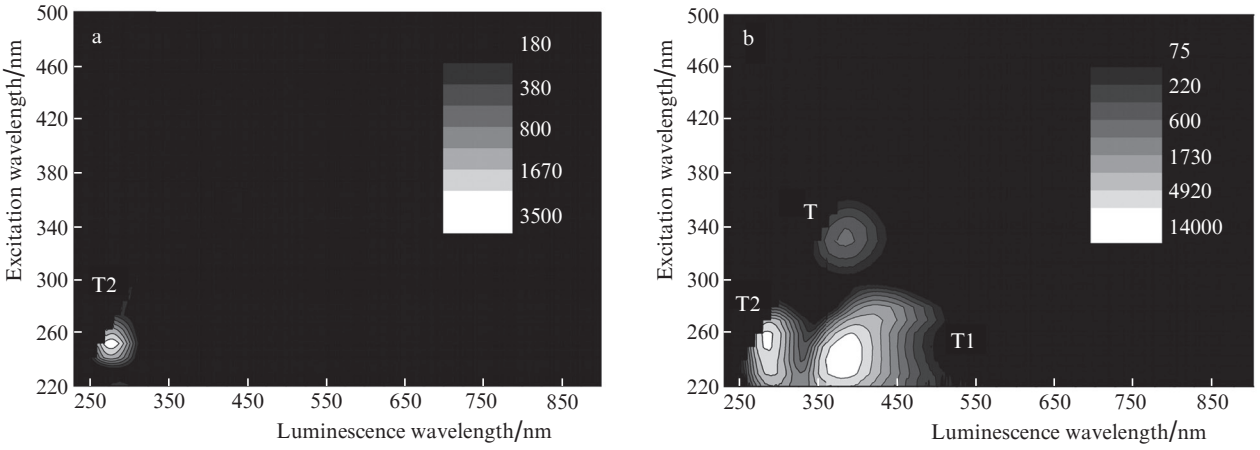

Figure 2. Luminescence spectra of bismuth-free (a) pure silica and (b) germanosilicate glass preforms. Here and in what follows, the luminescence intensity in 3D spectra is indicated in arbitrary units.

3.2. UV luminescence properties of the BACs

We studied in detail the luminescence properties of the BACs in silica fibres containing not only bismuth but also Al, P and Ge. $I_{lum}(\lambda_{ex}, \lambda_{em})$ luminescence spectra were constructed for the samples indicated in Table 1 and two bismuth-free samples (not indicated in Table 1).

Fibre with a bismuth-doped silica core. It is known that UV irradiation of glass may excite luminescence due to the presence of intrinsic defects in the glass network. To eliminate ambiguity in the assignment of peaks corresponding to BACs or intrinsic defects, we measured 3D spectra of samples identical in composition, one doped with bismuth and the other not. Figure 2a shows such a luminescence spectrum of a pure silica preform. The spectrum has only one luminescence peak, labelled T2 (λ_{ex} = 252 nm, λ_{em} = 279 nm). This peak is due to the singlet–singlet transition of a silicon-related oxygen-deficient centre (SODC) [19, 20]. No luminescence due to the triplet–singlet transition of this centre (excitation at 252 nm and luminescence at 460 nm) was detected in our experiments, because the oscillator strength of this transition is seven orders of magnitude lower than that of the singlet–singlet transition [19].

Figure 3a shows the 3D LS of the SBi sample (segments of the preform and fibre) in the range 240–1600 nm. At excitation wavelengths from 450 to 1600 nm, the 3D LS was measured previously using optical fibre [11]. In the range 240–450 nm, such spectra have been obtained for the first time. It is worth noting that the optical properties of such glasses and fibres have been the subject of extensive studies [10, 12, 14, 21]. Three groups of bands, A, B and C, are typical of Si-BACs, corresponding to luminescence wavelengths of 1410, 830 and 600 nm (Fig. 3a). Firstov et al. [11] detected peaks A, A1, A2, B and B1, as well as peak C, arising from divalent bismuth.

When luminescence was excited in the range 250–450 nm, we observed pairs of IR luminescence peaks (located on the same horizontal line): B2 (376 and 827 nm) + A3 (375 and 1417 nm) and B3 (~240 and 827 nm) + A4 (~240 and ~1417 nm) (Fig. 3a). From their position, we determined the energies of another two higher excited-state levels of the BACs (in addition to those known previously). Figure 3b shows the energy level diagram of the Si-BAC. The BAC lifetime was determined to be 640 μs at the SE_1 level, 40 μs at SE_2 and 3 μs at SE_3.

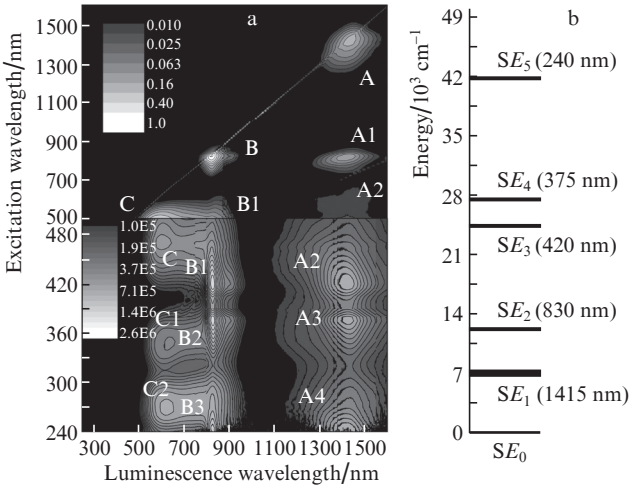

Figure 3. (a) Luminescence spectrum of the BACs in the SBi sample and (b) energy level diagram of a silicon-associated BAC.

The IR luminescence is accompanied by red luminescence [peaks C (470 and 603 nm), C1 (348 and 635 nm) and C2 (270 and 623 nm)], whose excitation spectrum is inconsistent with the above energy level diagram of the Si-BAC, in contrast to those of the groups of peaks A and B. This suggests that the IR luminescence differs in origin from the red luminescence. As shown earlier [11], the excitation spectra of the red luminescence (lifetime from 3 to 5 μs) are similar to those of divalent bismuth ions in crystals [22–24]. This leads us to conclude that the luminescence peaks C–C2 in Fig. 3a correspond to Bi^{2+} luminescence.

Table 2 lists the λ_{ex} and λ_{em} values corresponding to the luminescence peaks of the SBi sample at excitation wavelengths from 240 to 500 nm. The luminescence peak positions of this sample for $\lambda_{ex} \geqslant 450$ nm can be found in Ref. [11].

Fibre with a bismuth-doped germanosilicate glass core. It is known that UV excitation of bismuth-free germanosilicate glass often leads to bright blue luminescence, due to the presence of GODCs in the glass. The blue emission from such glasses can readily be observed by the naked eye. Figure 2b shows the $I_{lum}(\lambda_{em}, \lambda_{ex})$ luminescence spectrum of a sample identical in composition to GSBi (Table 1) but free of bismuth.

Table 2. Main luminescence peaks of the SBi sample (Fig. 3a) in the range 240 nm $\leqslant \lambda_{ex} \leqslant$ 500 nm.

Luminescence peak	λ_{ex}/nm	λ_{em}/nm
A2	422	1417
A3	375	1417
A4	~240	~1417
B1	421	827
B2	376	827
B3	~240	827
C	470	603
C1	348	635
C2	270	623

The luminescence of the GODCs has three strong peaks (about one order of magnitude brighter than the luminescence of the SODCs in Fig. 2a): T (333 and 384 nm), T1 (242 and 382 nm) and T2 (255 and 286 nm). The structure and optical properties of the GODCs have been investigated in sufficient detail in many studies (see e.g. Refs [16, 19]). The luminescence peaks T and T1 are known to arise from the triplet–singlet transitions and peak T2 is due to the singlet–singlet transition of the GODCs. In our experiments, peaks T2 and T1 were comparable in luminescence intensity, which was about three times the intensity of peak T.

The $I_{lum}(\lambda_{em}, \lambda_{ex})$ luminescence spectrum of the GSBi glass (Fig. 4a) contains much more luminescence bands than does the spectrum of SBi (Fig. 3a). First, there are all the luminescence peaks of the Si-BACs (A and B series). This is not unexpected because the core of the GSBi preform and fibre contains a large amount of SiO_2. Second, as shown by Firstov et al. [11] the fibre with the germanate core (consisting largely of GeO_2) has a system of luminescence peaks of Ge-BACs similar to that of the Si-BACs. However, only some of them are seen in Fig. 4a: BG, BG1 and AG2. It seems likely that, because of the relatively low GeO_2 concentration in our fibre, the intensity of peaks AG and AG1 (whose position in Fig. 4a is indicated according to Firstov et al. [11]) was insufficient for detection with respect to brighter luminescence. Also seen in Fig. 4a are the luminescence peaks BG2, BG3, AG3 and AG4, which have not been observed previously and, judging from the position of the luminescence bands, also arise from

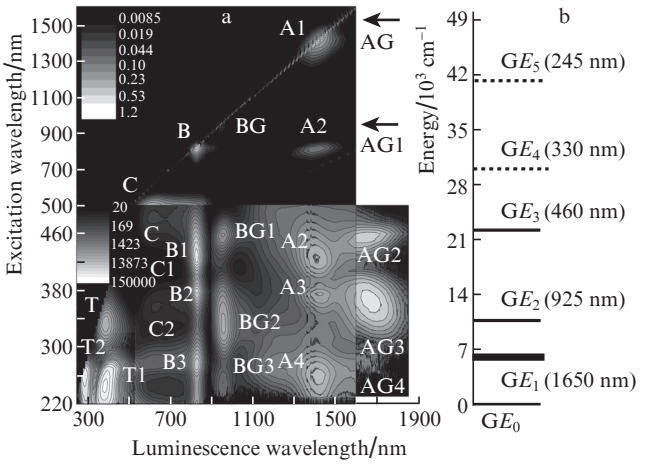

Figure 4. (a) Luminescence spectrum of the BACs in the GSBi sample and (b) energy level diagram of a germanium-associated BAC.

the Ge-BACs. It is worth noting that the presence of the strong absorption line of the GODCs in the GSBi fibre [16] (and their blue luminescence) may lead to a shift of the observed position of the luminescence peaks along the λ_{ex} axis. In particular, the λ_{ex} of peak B3 for the GSBi fibre is observed to be shifted by 30 nm to longer wavelengths relative to peak B3 in the SBi pure silica fibre (from ~240 nm for SBi to ~270 nm for GSBi).

Third, like that of the SBi fibre, the luminescence spectrum of the GSBi fibre contains a series of red luminescence peaks (C, C1 and C2), which arise from divalent bismuth luminescence, but in the case of GSBi their relative intensity is considerably lower. It is therefore reasonable to assume that, with increasing germanium oxide concentration, the divalent bismuth concentration decreases, especially because fibre with a bismuth-free germanate core showed no red luminescence [11]. From the data in Fig. 4a, we can approximately determine the position of two more energy levels of the Ge-BACs, but with considerably lower accuracy because of the effect of GODC bands. The energy level diagram obtained for the GODCs is presented in Fig. 4b (the dashed lines represent the levels whose position was determined with lower accuracy compared to the others because of the GODC position). As pointed out above, whereas the standard accuracy in the position of levels in our experiments is determined essentially by the λ_{ex} scan step (10 nm) in measurements of luminescence spectra, the error in the case of the GE_4 and GE_5 levels (Fig. 4b) may be several times greater.

Finally, in common with Fig. 2b, Fig. 4a shows three GODC luminescence peaks (T series).

Table 3 lists the λ_{ex} and λ_{em} values corresponding to the luminescence peaks of the GSBi sample at excitation wavelengths from 240 to 500 nm (the luminescence peak positions of this sample for $\lambda_{ex} \geqslant 450$ nm can be found in Ref. [11]).

Table 3. Main luminescence peaks of the GSBi sample (Fig. 4a) in the range 240 nm $\leqslant \lambda_{ex} \leqslant$ 500 nm.

Luminescence peak	λ_{ex}/nm	λ_{em}/nm
AG2	455	1646
AG3	365	1665
BG1	460	956
BG2	333	956
BG3	~247	956
T	333	387
T1	244	387
T2	260	290

It is of interest to note that the positions of the levels of both the Si-BACs and Ge-BACs meet the relation $E_2 - E_0 \approx E_3 - E_2$, i.e. the energy of the third excited state level is approximately twice that of the second level [25].

Fibres with bismuth-doped phosphosilicate and aluminosilicate glass cores. The luminescence spectra of the PSBi and ASBi samples (Figs 5a, 6), codoped with bismuth and phosphorus or aluminium, differ qualitatively from those of the SBi and GSBi samples (Figs 3a, 4a). In particular, Fig. 3a shows a system of luminescence peaks arranged in the form of a trapezium (A–A4 and B–B3) and having the same excitation wavelength in pairs (except for the 'unpaired' peak A). Such a luminescence spectrum allows one to uniquely determine the position of the energy levels of the Si-BACs. The luminescence spectra of PSBi and ASBi have no such system.

In the PSBi sample, the IR luminescence in the range near 1250–1300 nm is excited at several wavelengths starting at about 250 nm (luminescence peaks I–I5). There are also peaks B–B3. Their position suggests that these peaks are due to the Si-BACs. The 760-nm luminescence (peak C) corresponds to divalent bismuth [11]. Peak C1 (λ_{em} = 757 nm), lying on the same vertical as peak C, is probably also due to divalent bismuth luminescence under UV excitation. In addition, there is UV luminescence: peak Q at λ_{em} = 360 nm. Its λ_{ex} and λ_{em} correspond to the $^3P_1 \rightarrow {}^1S_0$ luminescence of the Bi^{3+} ion. This was described previously for glasses and crystals [26, 27]. Finally, there are luminescence peaks F–F2, similar in position to peaks B–B3 (it may be that peak F3, an analogue of peak B3, cannot be detected because of the presence of the strong peak C1).

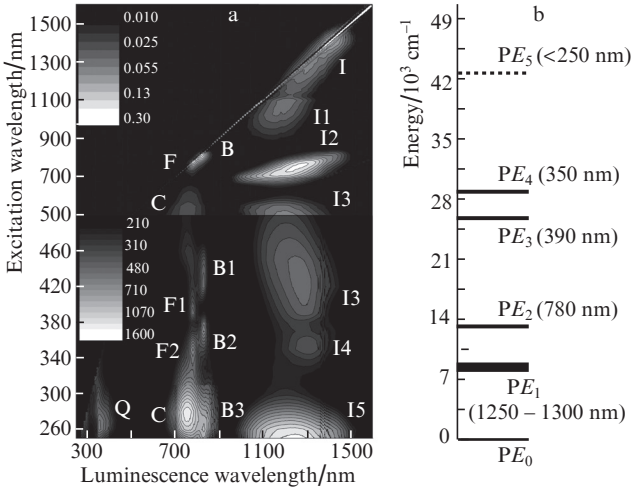

Figure 5. (a) Luminescence spectrum of the BACs in the PSBi sample and (b) energy level diagram of a phosphorus-associated BAC.

Assuming that the P-BACs are somewhat similar in structure to the Si-BACs and Ge-BACs, we can evaluate the energies of the second, third and fourth excited states of the P-BACs from the excitation wavelengths of peaks F–F2. The position of the first excited state of the P-BACs can be estimated from both the position of band I (Fig. 5a) and the lasing wavelength range of the P-BACs [28]. The position of the fifth energy level of the P-BACs can be assessed from the excitation wavelength of the IR emission band I5. The resultant energy level diagram of the P-BACs is presented in Fig. 5b. Note that, in common with the energy level diagrams of the Si-BACs and Ge-BACs, this diagram meets the relation $2PE_2 \approx PE_3$. Clearly, at the present stage this diagram should be regarded only as a first approximation for describing the levels of the P-BACs, as suggested by the complex IR luminescence excitation spectrum in the range 1–1.5 μm.

Table 4 lists the λ_{ex} and λ_{em} values corresponding to the luminescence peaks of the PSBi sample at excitation wavelengths from 240 to 500 nm (the luminescence peak positions of this sample for $\lambda_{ex} \geqslant 450$ nm can be found in Ref. [11]).

The luminescence spectrum of ASBi under UV excitation is considerably less informative than the spectra of the samples considered above. Figure 6 shows band C″, which has a luminescence wavelength close to the λ_{em} of band C′ and can be assigned to the luminescence of divalent bismuth in an aluminosilicate host [11]. Moreover, the shift of λ_{ex} to shorter

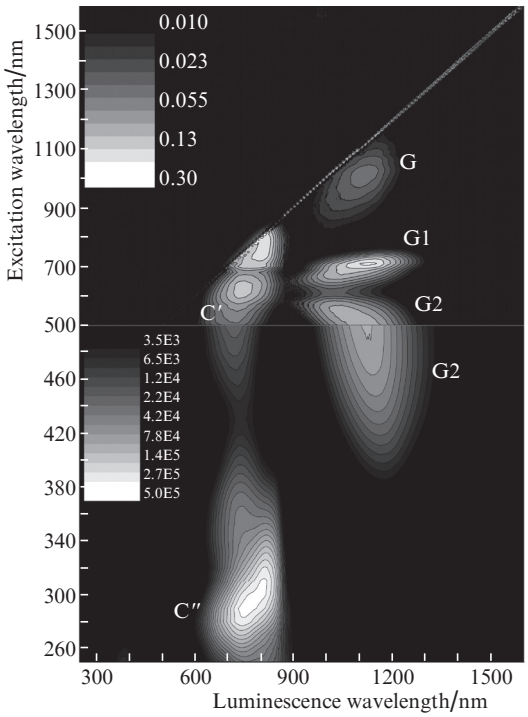

Figure 6. Luminescence spectrum of the BACs in the ASBi sample.

Table 4. Main luminescence peaks of the PSBi sample (Fig. 5a) in the range 240 nm $\leqslant \lambda_{ex} \leqslant$ 450 nm.

Luminescence peak	λ_{ex}/nm	λ_{em}/nm
I3	427	1277
I4	353	1300
I5	~250	~1250
F1	390	783
F2	350	783
C1	278	757
Q	265	360

wavelengths allowed us to record the entire peak G2 (in contrast to previous studies [11]). We found that, at the same sensitivity of the detection channel as in the case of SBi (Fig. 3a), GSBi (Fig. 4a) and PSBi (Fig. 5a), the ASBi samples showed no luminescence with $\lambda_{em} > 1$ μm under UV excitation.

Table 5 lists the λ_{ex} and λ_{em} values corresponding to the luminescence peaks of the PSBi sample at excitation wavelengths from 240 to 500 nm (the luminescence peak positions of this sample for $\lambda_{ex} \geqslant 450$ nm can be found in Ref. [11]).

Table 5. Main luminescence peaks of the ASBi sample (Fig. 6) in the range 240 nm $\leqslant \lambda_{ex} \leqslant$ 500 nm.

Luminescence peak	λ_{ex}/nm	λ_{em}/nm
G2	510	1100
C″	297	780

4. Discussion

It follows from the present results that the near-IR-emitting bismuth centres can be excited by UV radiation. The characteristic IR luminescence bands are then well seen in the spec-

tra of the SBi, GSBi and PSBi glasses. In contrast, ASBi shows no IR luminescence under UV excitation. Given that UV radiation is effectively absorbed in all the glasses under consideration, this suggests that nonradiative BAC relaxation processes play an important role in the ASBi sample.

The UV Bi^{3+} luminescence observed in PSBi (peak Q) was not detected in the SBi or ASBi sample but possibly took place in GSBi: there was a strong GODC luminescence peak in nearly the same region of the luminescence spectrum (Fig. 4a).

As to the IR luminescence, it is of interest to compare the UV absorption spectra of the samples under consideration (Fig. 1) to their IR luminescence excitation spectra. To extend the spectral range to 200 nm and improve the sensitivity of the detection channel, luminescence excitation spectra were measured at a signal acquisition time about two orders of magnitude longer than that in the case of the 3D luminescence spectra (Fig. 7). Also shown for comparison in Fig. 7 are the absorption spectra of the samples. The 1410- and 830-nm luminescence excitation spectra of the SBi sample differ little from its absorption spectrum. The luminescence excitation spectrum of the PSBi sample has a more complex structure than does its absorption spectrum, but on the whole it is also similar to the absorption spectrum. Finally, the luminescence excitation spectrum of ASBi has a large dip at 270 nm, indicative of nonradiative relaxation. At the same time, there is a rise at $\lambda_{ex} \approx 220$ nm in the excitation spectrum of the luminescence at $\lambda_{em} = 1150$ nm (Al-BAC luminescence). Therefore, the three samples (SBi, PSBi and ASBi) exhibit IR luminescence in bands corresponding to BACs under excitation at the absorption wavelengths of the Bi^{3+} ion. This suggests that Bi^{3+} participation in BAC formation cannot be ruled out. In particular, it is necessary to examine the possibility of BAC formation based on a Bi^{3+} ion and an oxygen-deficient centre in the glass host (since oxygen deficiency is a necessary condition for BAC formation [21]). Note that possible Bi^{3+} participation in BAC formation was examined previously in Refs [29] (where Bi^{3+} was a component of a Bi_2^{5+} dimer) and [30] (as a component of a $Bi^{3+} + Bi^{2+}$ dimer separated by an anion vacancy).

Thus, we have obtained excitation–emission spectra of bismuth-doped silica glasses, including those additionally doped with germanium, phosphorus or aluminium oxide. We have determined the position of the first five excited state energy levels of the Si-BACs and Ge-BACs. A tentative energy level diagram of the P-BACs has been proposed. The similarity between the IR luminescence excitation spectra and the UV absorption spectra of Bi^{3+} suggests that Bi^{3+} may participate in BAC formation, together with an oxygen-deficient defect of the glass host.

Acknowledgements. This work was supported in part by the Russian Foundation for Basic Research (Grant No. 13-02-01320) and the RF President's Grants Council (Support to the Leading Russian Scientific Schools Programme, Grant No. NSh-6653.2014.2).

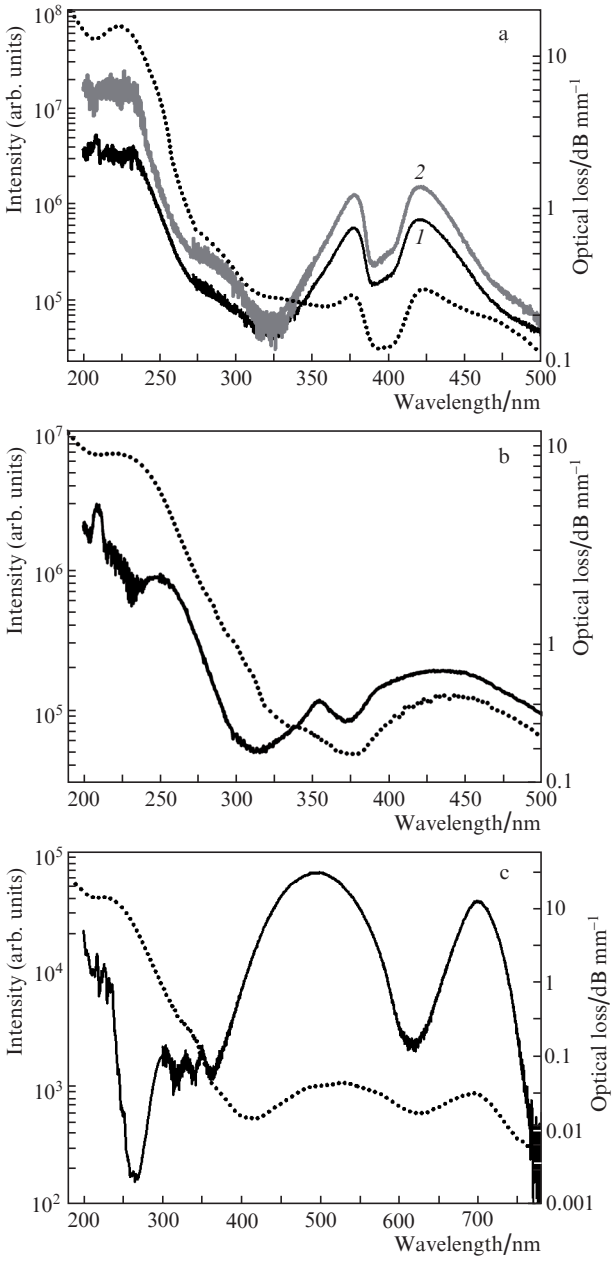

Figure 7. IR luminescence excitation (solid lines) and optical loss (dotted lines) spectra of (a) SBi [λ_{em} = (*1*) 1410 and (*2*) 830 nm], (b) PSBi (λ_{em} = 1250 nm) and (c) ASBi (λ_{em} = 1150 nm).

References

1. Dianov E.M. *Kvantovaya Elektron.*, **42** (9), 754 (2012) [*Quantum Electron.*, **42** (9), 754 (2012)].
2. Dianov E.M. *J. Lightwave Technol.*, **31** (4), 681 (2013).
3. Dianov E.M., Firstov S.V., Alyshev S.V., Riumkin K.E., Shubin A.V., Khopin V.F., Gur'yanov A.N., Medvedkov O.I., Mel'kumov M.A. *Kvantovaya Elektron.*, **44** (6), 503 (2014) [*Quantum Electron.*, **44** (6), 503 (2014)].
4. Bufetov I.A., Melkumov M.A., Khopin V.F., Firstov S.V., Shubin A.V., Medvedkov O.I., Guryanov A.N., Dianov E.M. *Proc. SPIE Int. Soc. Opt. Eng.*, **7580**, 758014 (2010).
5. Melkumov M.A., Bufetov I.A., Shubin A.V., Firstov S.V., Khopin V.F., Guryanov A.N., Dianov E.M. *Opt. Lett.*, **36** (13), 2408 (2011).
6. Riumkin K.E., Melkumov M.A., Bufetov I.A., Shubin A.V., Firstov S.V., Khopin V.F., Guryanov A.N., Dianov E.M. *Opt. Lett.*, **37** (23), 4817 (2012).
7. Riumkin K.E., Mel'kumov M.A., Shubin A.V., Firstov S.V., Bufetov I.A., Khopin V.F., Gur'yanov A.N., Dianov E.M. *Kvantovaya Elektron.*, **44** (7), 700 (2014) [*Quantum Electron.*, **44** (7), 700 (2014)].
8. Peng M., Wang C., Chen D., Qiu J., Jiang X., Zhu C. *J. Non-Cryst. Solids*, **351**, 2388 (2005).

9. Khonthon S., Morimoto S., Arai Y., Ohishi Y. *Opt. Mater*., **31**, 1262 (2009).
10. Neff M., Romano V., Luethy W. *Opt. Mater*., **31**, 247 (2008).
11. Firstov S.V., Khopin V.F., Bufetov I.A., Firstova E.G., Guryanov A.N., Dianov E.M. *Opt. Express*, **19** (20), 19551 (2011).
12. Razdobreev I., El Hamzaoui H., Ivanov V.Yu., Kustov E.F., Capoen B., Bouazaoui M. *Opt. Lett*., **35** (9), 1341 (2010).
13. Dvoyrin V.V., Medvedkov O.I., Mashinsky V.M., Umnikov A.A., Guryanov A.N., Dianov E.M. *Opt. Express*, **16**, 16971 (2008).
14. Bufetov I.A., Semenov S.L., Vel'miskin V.V., Firstov S.V., Bufetova G.A., Dianov E.M. *Kvantovaya Elektron*., **40** (7), 639 (2010) [*Quantum Electron*., **40** (7), 639 (2010)].
15. Zlenko A.S., Dvoyrin V.V., Mashinsky V.M., Denisov A.N., Iskhakova L.D., Mayorova M.S., Medvedkov O.I., Semenov S.L., Vasiliev S.A., Dianov E.M. *Opt. Lett*., **36** (13), 2599 (2011).
16. Neustruev V.B. *J. Phys. Condens. Matter*, **6**, 6901 (1994).
17. Oboth K.P., Lonmeier F.J., Fischer F. *Phys. Status Solidi B*, **154**, 789 (1989).
18. Duffy J.A. *J. Chem. Educ*., **73** (12), 1138 (1996).
19. Skuja L. *J. Non-Cryst. Solids*, **16**, 239 (1998).
20. Griscom D.L. *J. Ceram. Soc. Jpn*., **99** (10), 923 (1991).
21. Zlenko A.S., Mashinsky V.M., Iskhakova L.D., Semjonov S.L., Koltashev V.V., Karatun N.M., Dianov E.M. *Opt. Express*, **20** (21), 23186 (2012).
22. Peng M., Wondraczek L. *J. Am. Ceram. Soc*., **93** (5), 1437 (2010).
23. Gaft M., Reisfeld R., Panczer G., Boulon G., Saraidarov T., Erlish S. *Opt. Mater*., **16** (1-2), 279 (2001).
24. Srivastava A.M. *J. Lumin*., **78** (4), 239 (1998).
25. Firstov S.V., Khopin V.F., Velmiskin V.V., Firstova E.G., Bufetov I.A., Guryanov A.N., Dianov E.M. *Opt. Express*, **21** (15), 18408 (2013).
26. Parke S., Webb R.S. *J. Phys. Chem. Solids*, **34**, 85 (1973).
27. Zorenko Yu., Gorbenko V., Voznyak T., Vistovsky V., Nedilko S., Nikl M. *Radiat. Meas*., **42**, 882 (2007).
28. Bufetov I.A., Firstov S.V., Khopin V.F., Medvedkov O.I., Guryanov A.N., Dianov E.M. *Opt. Lett*., **33** (19), 2227 (2008).
29. Denker B.I., Galagan B.I., Osiko V.V., Shulman I.L., Sverchkov S.E., Dianov E.M. *Appl. Phys. B*, **98**, 455 (2010).
30. Dianov E.M. *Kvantovaya Elektron*., **40** (4), 283 (2010) [*Quantum Electron*., **40** (4), 283 (2010)].